Dynamic magnetic anisotropy at the onset of exchange bias: The NiFe/IrMn ferromagnet/antiferromagnet system

Jeffrey McCord*
Leibniz Institute for Solid State and Materials Research IFW Dresden, Institute for Metallic Materials, Helmholtzstrasse 20, 01069 Dresden, Germany

Roland Mattheis
Institute for Physical High Technology IPHT Jena, Albert-Einstein-Strasse 9, 07745 Jena, Germany

Dieter Elefant
Leibniz Institute for Solid State and Materials Research IFW Dresden, Institute for Solid State Research, Helmholtzstrasse 20, 01069 Dresden, Germany

(Received 26 April 2004; published 27 September 2004)

The strength of exchange bias and rotatable anisotropy in polycrystalline NiFe−IrMn ferromagnet/antiferromagnet systems is quantified from dc down to the picosecond time scale by regular quasistatic and microwave magnetometry, as well as magnetic domain observation. A transition from superparamagnetic to antiferromagnetic behavior with increasing IrMn thickness is derived from the magnetic resonance frequency and the effective magnetic damping parameter. A discrepancy between magnetic loop shift and dynamically obtained exchange bias strength is explained by asymmetric rotatable anisotropy contributions with different relaxation times in the antiferromagnetic layer. The time-dependent relaxation is directly confirmed by magnetic domain observations. Partially switching in the IrMn layer even with strong exchange bias is concluded. The increase of coercivity rises solely from the rotatable anisotropy contribution.

DOI: 10.1103/PhysRevB.70.094420 PACS number(s): 75.70.Cn, 75.70.Kw, 75.60.−d, 75.50.Ee

I. INTRODUCTION

The interfacial exchange coupling[1] between the spins of a ferromagnetic (F) layer and an antiferromagnetic (AF) layer has been extensively investigated in the past years. Reviews on exchange bias can be found in Refs. 2–5. Experimentally, the exchange bias phenomenon manifests itself in a field shift of the magnetic hysteresis loop, referred to as the exchange bias field H_{eb}, and an increase of coercivity H_c measured in the F film. Numerous theories have been developed that predict values for H_{eb} in reasonable agreement with experimental results. The models[6–14] consider compensated or uncompensated interfaces, polycrystalline thin-film systems, spin-flop coupling, and interface roughness. The internal AF grain and domain structure add many additional aspects to the exchange bias phenomena.

Several mechanisms have been proposed to explain the enhanced H_c in F/AF bilayers. Models include FM domain wall pinning at AF domains[15] and other F/AF interactions.[16,17] Particularly, time-dependent effects are reported in F/AF systems related to thermally activated switching of AF grains. McMichael *et al.*[18] connected the exhibited rotatable anisotropy H_{rot} (Ref. 19) to changes in the antiferromagnetic domain structure. This anisotropy can be understood as an anisotropy that has an energetic minimum which aligns parallel to a (possibly changing) F layer magnetization direction. It is related to irreversible changes in the AF layer and should not be confused with stripe domain effects observed in out-of-plane anisotropy films.[20] The phenomena can be modeled assuming two components in the AF layer.[2,21,22] When changing the magnetic state of the ferromagnetic layer, one part of the AF grains follows the F layer magnetization, leading to a rotatable anisotropy contribution. The other is fixed, not following the F magnetization, therefore resulting in exchange bias. Obviously related is the training effect,[23,24] manifesting itself in changes in the hysteretic characteristics depending on magnetic history. These effects become most pronounced for thin AF layers,[25–27] where enhanced uniaxial anisotropy effects are reported. A detailed discussion on the various aspects of rotatable anisotropy, the related enhancement of uniaxial anisotropy, and the training effect can be found in the introduction of Ref. 22.

In the present paper we separate the rotatable and the unidirectional anisotropy contributions with varying AF layer thickness by complementary dc and rf measurements. We focus on time-dependent relaxation effects in the AF, important for understanding of the F/AF magnetic structure. The stability of exchange bias and rotatable anisotropy is probed by different techniques. The discussed results are relevant for the understanding of exchange bias in polycrystalline thin films.

II. SAMPLE PREPARATION

Magnetic bilayer $Si/SiO_2/Ta(5\ nm)/Ni_{81}Fe_{19}(40\ nm)/Ir_{22}Mn_{78}(0.2\ nm \ldots 9\ nm)/Ru(3\ nm)$ structures are prepared by dc-magnetron sputtering in a multitarget UHV sputter system with a base pressure below 2×10^{-8} Torr at an Ar pressure of 5×10^{-3} Torr. The Ta seed layer insures good $\langle 111\rangle$ texture. The distribution of texture is within $\sigma=6\%$ and the grain size is typically distributed tightly around d_{grain}

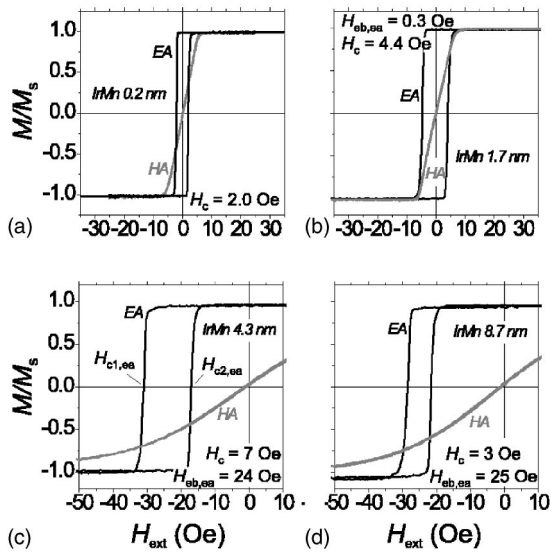

FIG. 1. Hysteresis loops along the easy (EA) and hard axis (HA) of selected F/AF structures. The AF film thickness is (a) 0.2 nm, (b) 1.7 nm, (c) 4.3 nm, and (d) 8.7 nm. The coercivity field $H_{c,ea}$ and the loop shift $H_{eb,ea}$ is indicated.

=15 nm.[28] The F uniaxial anisotropy axis and the initial exchange bias direction are set in an applied magnetic in-plane field of $H_{dep}=50$ Oe during film deposition. The top Ru layer prevents corrosion of the F/AF stack. No postannealing processing steps are done.

III. MAGNETIC CHARACTERIZATION

The films are characterized by inductive magnetometry with a field sweep rate of 10 Hz. The exchange bias field $H_{eb,ea}$ is obtained from the loop shift $(H_{c2,ea}-H_{c1,ea})/2$ along the magnetically easy axis (EA, parallel to H_{dep}). The measuring field was aligned with an accuracy of 2° relative to the EA. Example loops are shown in Fig. 1. For the thinnest IrMn layer thickness ($t_{IrMn}=0.2$ nm) a regular hysteresis loop with no influence of the AF layer on the magnetic properties is obtained. With increasing AF film thickness ($t_{IrMn}=1.7$ nm) an increase in coercivity along the EA is seen. With again increasing AF layer thickness, shown is $t_{IrMn}=4.3$ nm, $H_{eb,ea}$ appears. Beyond that ($t_{IrMn}=8.7$ nm), $H_{eb,ea}$ stays nearly constant, but the coercivity reduces again. However, the obtained coercivity values are still larger than the initial FM coercivity.

As in regular hysteresis loop measurements along the easy or hard axis the rotatable anisotropy field is not easily accessible, a complementary more detailed analysis by pulsed inductive micrometer magnetometry (PIMM) (Ref. 29) with varying bias field H_{bias} is performed. Using large bias fields, coercivity effects can be eliminated. In addition, varying H_{bias} allows an independent extraction of the exchange bias field $H_{eb,dyn}$ and the rotatable anisotropy field $H_{rot,dyn}$ as will be outlined below. A sketch of the experimental geometry is given in Fig. 2. $H_{rot,dyn}$ follows the direction of magnetization [compare Figs. 2(a) and 2(b)]. As the measurement takes place on the nanosecond timescale, the rotatable anisotropy

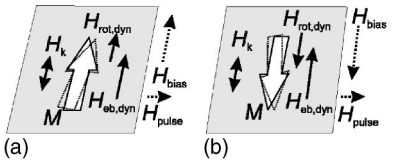

FIG. 2. Schematic drawing of the experimental geometry. The directions of acting fields are display for two exemplary cases.

part in the AF does not respond to the exciting fast rise time pulse field ($t_{rise\ time}<100$ps, $H_{pulse}\approx 5$ Oe), which is aligned perpendicular to the effective anisotropy and parallel oriented bias field H_{bias}. $H_{rot,dyn}$ then acts similar as a uniaxial anisotropy field H_k. Moreover, the effective magnetic damping parameter α_{eff} is extracted. From α_{eff} conclusions about inhomogeneities in the F/AF structure[18] and the paramagnetic-antiferromagnetic transition with AF layer thickness can be obtained.[30] In addition, the technique acts similar to a transverse ac-susceptibility measurement,[31–33] thus eliminating coercivity effects in the F/AF bilayer system.

Selected PIMM data from the same IrMn thickness as in Fig. 1 for $H_{bias}=-20$ Oe is displayed in Figs. 3(a), 3(c), and 3(e) (left column). Besides the change in the ferromagnetic resonance frequency f_{res}, differences in α_{eff} (visible from the exponential decay time τ of the voltage signal) becomes evident. In our time-domain analysis we derive α_{eff} using

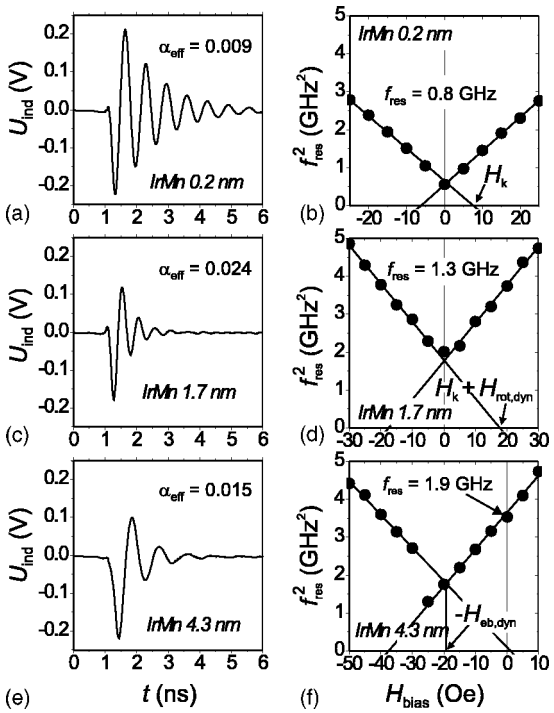

FIG. 3. Example PIMM data for an bias field $H_{bias}=-20$ Oe applied along the induced anisotropy axis (left column) and change of f_{res}^2 with H_{bias} (right column). All measurements were done after saturation in a positive field. From the linear interpolation $H_{eb,dyn}$ and the sum of H_k and $H_{rot,dyn}$ is derived. α_{eff} and zero field f_{res} ($H_{bias}=0$ Oe) values are shown. The AF film thickness is (a) and (b) 0.2 nm, (c) and (d) 1.7 nm, (e) and (f) 4.3 nm, respectively (as indicated).

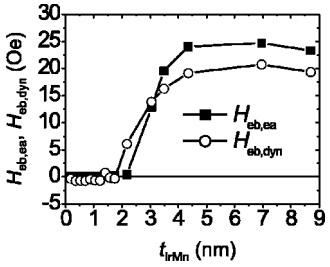

FIG. 4. EA loop shift $H_{eb,ea}$ and $H_{eb,dyn}$ from the horizontal frequency shift as a function of t_{IrMn}.

$$\alpha_{eff} = \frac{2}{\tau\gamma\mu_0 M_s} \tag{1}$$

with the saturation magnetization M_s ($M_{s,NiFe}$=800 kA/m), the permeability μ_0 ($4\pi\times10^{-7}$ Vs/Am), and the gyromagnetic ratio γ ($\gamma/2\pi$=1.8 T^{-1} s^{-1}). This approximation is adequate for our purpose.[34] The change of ferromagnetic resonance frequency with external bias field H_{bias} is analyzed using the modified Kittel's equation,[35] including the rotatable anisotropy field $H_{rot,dyn}$ and the exchange bias field $H_{eb,dyn}$. Taking the effective fields acting in the F/AF stack into account, Kittel's equation can be written as

$$f_{res} = \frac{\gamma\mu_0}{2\pi}\sqrt{M_s(H_k + H_{rot,dyn}) + M_s(H_{eb,dyn} + H_{bias})} \tag{2}$$

for $H_{eb,dyn}+H_{bias}\geqslant 0$, and

$$f_{res} = \frac{\gamma\mu_0}{2\pi}\sqrt{M_s(H_k + H_{rot,dyn}) - M_s(H_{eb,dyn} + H_{bias})} \tag{3}$$

for $H_{eb,dyn}+H_{bias}\leqslant 0$.

$H_{rot,dyn}$ adds to the effective anisotropy field and leads to an increase in f_{res}. From the extrapolation of f_{res}^2 to zero frequency, $H_{rot,dyn}$ can be extracted in the knowledge of H_k. In our case we derived H_k from the low AF-layer thickness and assumed it to be identical for all samples. Depending on the bias field value H_{bias} Eq. (2) (where the magnetization is aligned parallel to the exchange bias field), or Eq. (3) (for antiparallel alignment) is valid. $H_{eb,dyn}$ results in a horizontal shift of the f_{res} bias field dependency on H_{bias}. The minimum of f_{res}^2 with H_{bias} is at $-H_{eb,dyn}$. Experimental results of f_{res}^2 with H_{bias} for different samples are plotted in Figs. 3(b), 3(d), and 3(f) (right column). Comparing the linear f_{res}^2 dependence for t_{IrMn}=0.2 nm and t_{IrMn}=1.7 nm, the vertical resonance frequency shift due to $H_{rot,dyn}$ is evident. No exchange bias is noticeable. With further increasing AF-layer thickness the frequency plots are shifted to the left (t_{IrMn}=4.3 nm) by $H_{eb,dyn}$.

The change of exchange bias field $H_{eb,ea}$ with AF layer thickness, derived from the loop shift along EA, together with $H_{eb,dyn}$ are displayed in Fig. 4. Two results become obvious. First, the onset of exchange bias is shifted to smaller t_{IrMn} values in the dynamic case. Second, $H_{eb,dyn}$ is substantially smaller than $H_{eb,ea}$. A similar variance was found by ferromagnetic resonance analysis of exchange biased NiO-based F/AF bilayer structures[18] and explained by asymmetric hysteresis effects together with rotatable anisotropy contributions. (Note that Miltény *et al.*[36] have obtained contrary results for single-crystal Fe/FeF_2 F/AF structures, suggesting other or additional mechanisms involved there.)

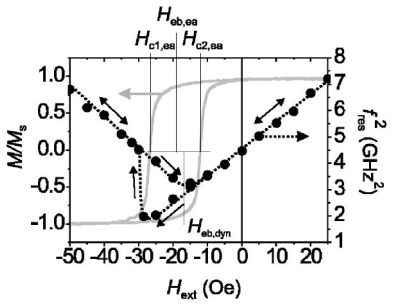

FIG. 5. EA loop together with f_{res}^2 as a function of applied external field. The position of $H_{eb,dyn}$, $H_{eb,ea}$, $H_{c1,ea}$, and $H_{c2,ea}$ are indicated. The field progression in the hysteretic regime is marked by arrows. The AF film thickness is t_{IrMn}=3.5 nm.

For clarification of the discrepancy between $H_{eb,ea}$ and $H_{eb,dyn}$ a direct comparison of hysteresis and resonance frequency dependence is plotted in Fig. 5. The resonance frequency f_{res} follows the Kittel dependency of Eq. (2) and Eq. (3) in the nonhysteretic regime. Due to the hysteretic magnetization process of the FAF layer system, the linear dependency of f_{res}^2 with H_{bias} extends across the H_{bias} limit of Eq. (2) and Eq. (3), respectively. Congruently with the hysteresis in magnetization, a hysteresis in the resonance frequency occurs. A linear interpolation of both branches of f_{res}^2 leads to an $H_{eb,dyn}$ closer to $H_{c2,ea}$. Deriving H_{eb}, under the assumption of a symmetric hysteresis loop around $H_{eb,ea}$, from the loop shift is apparently invalid. The ''real'' exchange bias field lies more closely to $H_{c2,ea}$. This also implies that the magnetization reversal along the EA occurs asymmetric relative to the exchange bias field. This is in agreement with magnetometry[37] and domain observations,[38,39] where a pronounced reversal asymmetry related to magnetization changes in the AF layer are reported. The origin of coercivity cannot be neglected to understand the difference between $H_{eb,ea}$ and $H_{eb,dyn}$.

The source for the enhanced $H_{c,ea}$ becomes clear by analyzing $H_{rot,dyn}$ and α_{eff} contributions plotted in Fig. 6. $H_{rot,dyn}$ and $H_{c,ea}$ change almost coincidental with AF layer thickness [Fig. 6(a)]. The concurrent onset, peak value, and decrease with further increasing IrMn thickness of both values indicates that the change of magnetization in the AF layer (the rotatable part) is the main source for the variation of coercivity with AF layer thickness. No correlation of coercivity with H_{eb} as proposed in Ref. 40 is apparent. The rotatable anisotropy part also reflects itself in the magnetic damping parameter α_{eff} [Fig. 6(b)]. For small AF layer thickness an onset of α_{eff} before $H_{eb,dyn}$ and $H_{rot,dyn}$ becomes visible. Above the onset of α_{eff} at t_{IrMn}=1.0 nm the AF layer is already antiferromagnetic in character and displays superparamagnetic behavior.

Steenbeck *et al.*[28] experimentally derived the antiferromagnetic anisotropy constant $K_{AF,IrMn}$ as a function of IrMn thickness at T=10 K. For t_{IrMn}=1.4 nm an AF anisotropy of $K_{AF,IrMn}=1.3\times10^4$ J/m^3 was obtained. Setting the limit for superparamagnetism at nanosecond time scale to

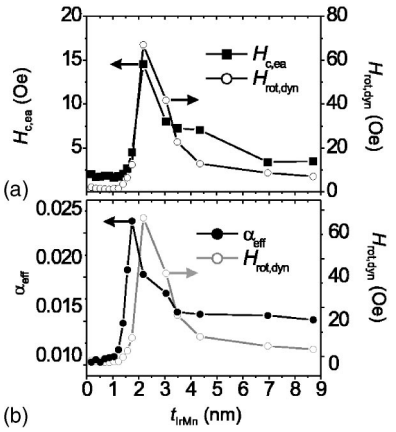

FIG. 6. (a) Change of $H_{\mathrm{rot,dyn}}$ and $H_{\mathrm{c,ea}}$, and (b) α_{eff} with t_{IrMn}.

$$K_{\mathrm{AF,IrMn}} V_{\mathrm{grain}} = k_{\mathrm{B}} T, \tag{4}$$

with the average grain volume $V_{\mathrm{grain}} = t_{\mathrm{IrMn}} r_{\mathrm{grain}}^2 \pi$ ($r_{\mathrm{grain}} = 7.5$ nm; see Sec. II), the Boltzmann constant $k_{\mathrm{B}} = 1.38 \times 10^{-23}$ J/K, and temperature $T = 300$ K, we obtain $K_{\mathrm{AF,IrMn}} = 1.4 \times 10^4$ J/m^3 for the superparamagnetic anisotropy limit in good agreement with the experimental value of $K_{\mathrm{AF,IrMn}}$. Note that Eq. (4) is only valid for uncoupled grains. The thermally activated switching of AF magnetization happens on the subnanosecond time scale, leading to enhanced magnetic damping[30] in the F/AF layer stack. A peak in α_{eff} occurs at $t_{\mathrm{IrMn}} \approx 1.7$ nm. The enhancement of magnetic damping happens well below the onset of exchange biasing and the increase of coercivity.

With increasing AF thickness, the anisotropy energy of the AF results in a stabilization of the AF magnetization on the nanosecond time scale. As a result, the rotatable anisotropy field $H_{\mathrm{rot,dyn}}$ starts to develop. With yet increasing IrMn thickness, the anisotropy stabilizes even more and exchange bias $H_{\mathrm{eb,dyn}}$ occurs on the time scale of the measurement. This development is supported by the fact that with increasing AF thickness, the AF interaction leads to an effective enlargement of the volume of the AF. In addition, a strong increase in AF anisotropy above $t_{\mathrm{IrMn}} = 2$ nm is found experimentally.[28]

The total anisotropy field, derived from $H_{\mathrm{total}} = H_{\mathrm{rot,dyn}} + H_{\mathrm{eb,dyn}}$, is plotted in Fig. 7. A strong increase with increasing IrMn layer thickness is seen. The maximum in the anisotropy field takes place close to $t_{\mathrm{IrMn}} = 2$ nm. With thicker AF layer thickness, H_{total} decreases again. Evidently, only taking the AF anisotropy or grain-size distribution into account[15–17,28,40] is not sufficient to describe the F/AF layer interaction properly. The rotatable anisotropy has a strongly time-dependent contribution, confirming the concept of thermally activated AF grain switching.[18] The sum of anisotropy fields displays a similar dependence as the exchange bias data presented in Refs. 27 and 41, but measured at a temperature of $T = 4$ K. This indicates that the frequently observed decrease in exchange bias with increasing temperature is related to the onset of thermally activated AF switching. For higher temperatures, exchange bias transforms into rotatable anisotropy, the exchange bias decreases congruently.

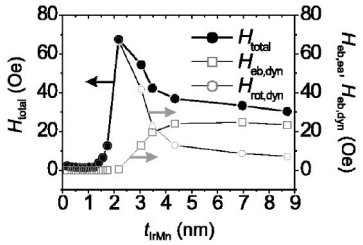

FIG. 7. (a) Total anisotropy field H_{total}, $H_{\mathrm{rot,dyn}}$, and $H_{\mathrm{eb,dyn}}$ as function of AF layer thickness t_{IrMn}.

From our data, both F/AF coupling effects, rotatable and unidirectional anisotropy, can be interpreted as unstable AF grain magnetization, just differing by deviating relaxation times. A continuous transition from rotatable to dominating unidirectional anisotropy is observed. Even for large AF layer thickness rotatable anisotropy contributions and therefore partially switching in the AF exists. The rotation of anisotropy, however, has also a strong influence on the remagnetization process at longer time scales, within and beyond the integration times of the measurement techniques used before, as shown in the following section.

IV. DOMAIN EFFECTS

In this section we focus on the magnetization process at one AF layer thickness ($t_{\mathrm{IrMn}} = 3$ nm), where rotatable and unidirectional anisotropy field are both of significant value. To obtain a better inside in the magnetization process, we imaged the magnetic domain structure by magneto-optical Kerr microscopy in the longitudinal mode. The domains in the F layer are visualized through the covering IrMn and Ru protection layer. The sweep rate during the observation can be varied continuously down to dc ($\delta H_{\mathrm{ext}}/\delta t = 0$). Applying a constant magnetic field, still within the coercivity range above $H_{\mathrm{c1,ea}}$, viscous remagnetization is observed. Results are displayed in Fig. 8.

Holding the field at $H_{\mathrm{ext}} = -20$ Oe, domain wall creeping over minutes in the F structure due to reversal in the AF layer is seen [Fig. 8(a)]. The remagnetization takes place mostly by domain wall motion together with incoherent rotation. The wall angle is not aligned parallel to the uniaxial anisotropy field of the F layer or the induced exchange bias direction of the F/AF system. As the domain wall orientation is determined by the direction of net magnetization during magnetization reversal, the tilted wall angle indicates a reorganization of the spins in the AF away from the anisotropy axis during magnetization switching of the F/AF system. In addition we observe memory effects in the F/AF layer structure, meaning that the domain structure during magnetization reversal is strongly dependent on the magnetic field and domain history of the sample. This indicates irreversible rearrangement of the AF spins influencing the domain structure during reversal, as will be discussed later in this article. A direct correlation between static AF and F domains was nicely demonstrated in Ref. 42. The whole magnetization

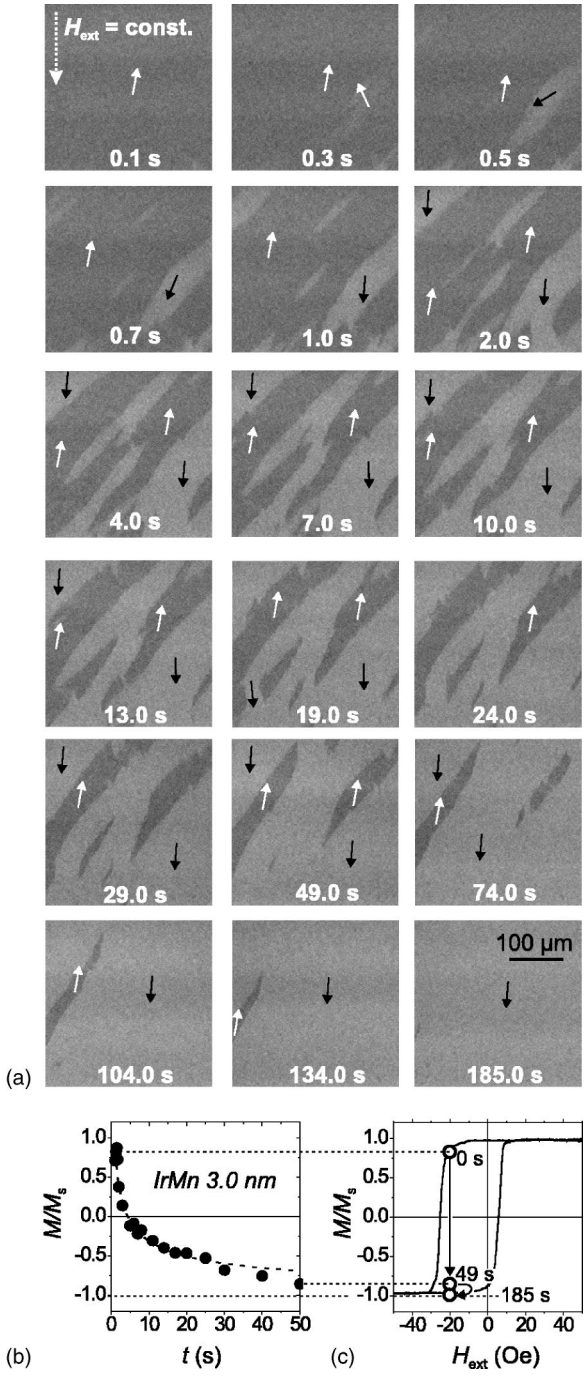

FIG. 8. (a) Magnetization reversal at *constant* applied field $H_{ext}=-20$ Oe. The IrMn thickness is 3.0 nm. The time of observation is indicated. Magnetization directions are sketched qualitatively. H_{ext} is above the coercivity $H_{c1,ea}\approx-25$ Oe. (b) Relative change of magnetization vs time corresponding to (a). (c) Hysteresis loop along EA. The development of the magnetization with time (0 s, 49 s, 185 s) is displayed (○).

process takes place over several minutes [Fig. 8(a), 0.1 s,…, 185 s]. A quantitative evaluation, directly derived from the magneto-optical images, is displayed in Fig. 8(b). A nearly exponential reversal in time is visible for the first seconds. The change of magnetization with time can be interpreted as a change in coercivity $H_{c1,ea}(t)$. For comparison the regularly

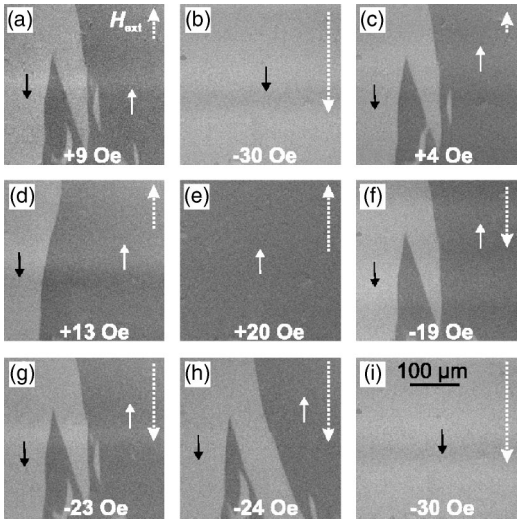

FIG. 9. (a) Initial domain configuration for the same sample as Fig. 8 ($t_{IrMn}=3.0$ nm) adjusted at constant field $H_{ext}=9$ Oe. (b)–(e) Domain formation during magnetization reversal for the forward branch of the loop after keeping the domain structure (a) for 5 h. (e)–(i) Magnetic microstructure at backward loop. Magnetization directions and applied field values are indicated. Total measuring time is about 1 min.

measured hysteresis loop along the EA is displayed in Fig. 8(c). The starting field ($t=0$ s) of the domain observation and the development of the magnetization with time is sketched in Fig. 8(c).

Another example of dynamic domain processes is shown in Fig. 9. After setting a domain structure [Fig. 9(a)] for 5 h, the AF magnetization in the F/AF stack stabilizes. During reversal the initiated domain structure reappears along both branches [Figs. 9(c) and 9(g)] of the magnetization loop. This is conclusive with a local change of loop shift. The slowly responding part of rotatable anisotropy, reversed within hours, results in a change of loop shift on the time scale of the domain observation of about 1 min. The slowly remagnetizing fraction of the AF layer does appear as an exchange bias contribution in the magnetometric measurements. Due to the shifted exchange bias in one of the domain regions relative to the other, the domain structure during reversal [Figs. 9(c) and 9(g)] is a copy of the formerly adjusted domain pattern [Fig. 9(a)]. The domain pattern exists over a certain field range [compare Fig. 9(c) with 9(d) and 9(f) with 9(g)]. The character of the domains is strongly influenced by the memory of the F/AF bilayer system due to the rotatable anisotropy in the AF layer. This also affects the Néel walls in the F layer, which will be partially fixed in the setting procedure [Fig. 9(a)] due to the viscous AF structure.

A quantitative confirmation of the observations is obtained from investigations on the same sample by alternating gradient magnetic force magnetometry. Experiments with different field history, latency between the measurements, and field sweep rates are performed. Exemplary data is shown in Fig. 10. During the time interval between the measurements creeping effects at remanent state are recorded and indicated in each figure. The field sweep rate of each loop measurement is displayed.

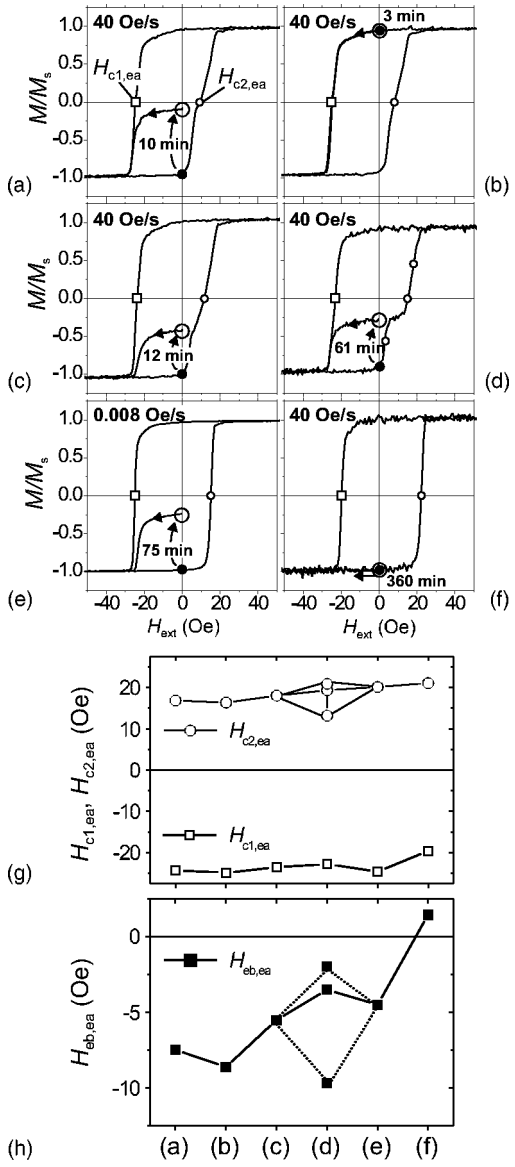

FIG. 10. (a) Magnetization reversal after setting the magnetization to remanent state in a field of $H_{ext}=-50$ Oe ($t_{IrMn}=3.0$ nm). Reversal after applying (b) $H_{ext}=500$ Oe and (c) $H_{ext}=-3000$ Oe. The time between the loop measurements is below 10 min. Relative starting times t are indicated. (d) Loop after setting the magnetization for 1 h after measuring (c). (e) Sequencing reversal with extremely slow low field sweep rate. (f) Fast reversal after (e). The field sweep rates f_{meas} are indicated. The initial remanent states before loop measurements are marked by a ●, the starting point of the loop measurement by an open circle ○. The corresponding values of $H_{c1,ea}$, $H_{c2,ea}$ are plotted in (g). $H_{eb,ea}$ is shown in (h). For the data corresponding to (d) more than one set of data is displayed, reflecting the pronounced bimodal state of the sample.

Before the measurement [Fig. 10(a)] a negative magnetic field was applied (the high remanent state is marked by ●). Due to the viscous character of the AF a reduction in remanence (○) is observed. Starting from the negative remanent point the magnetization decays as shown in Figs. 10(a) and 10(c)–10(e). (Note that the amount of decay is not only dependent on the waiting time, but also on the overall magnetic history.) Before the start of the loop measurement, a two domain state develops. As shown before [Fig. 9(a)] no change in field is necessary to partially reverse the magnetization in the F/AF bilayer. Beginning from the mixed domain state a small residual step close to $H_{c2,ea}$ is visible during magnetization reversal. With positive remanence no change in the spin structure in the AF becomes obvious due to the much larger amplitude of $H_{c1,ea}$ [Fig. 10(b)]. The reversal starts at the high remanent state. $H_{c2,ea}$ is slightly reduced relative to [Fig. 10(a)]. Changing the initial conditions back again [Fig. 10(c)], a similar behavior as in Fig. 10(a) is observed. Keeping the two domain state for a longer time ($t=61$ min), the step in the magnetization curve along the forward branch becomes more pronounced [Fig. 10(d)]. The reorganization of the AF layer due to the slowly rotating AF spins is more complete. Two different regions with different coercivity and loop shift are clearly visible [see Figs. 10(g) and 10(h) for values]. [This situation is similar to the condition in which 9(a) was adjusted]. The effective $H_{c2,ea}$ values for the lower and upper part of the loop branch are decreased and increased, respectively. The left branch of the loop displays almost no dependency on magnetic history. Only a slight decrease in coercivity is observed. Even measuring for several hours [Fig. 10(e)] no significant change of $H_{c1,ea}$ is seen. However, the initial value of coercivity of Fig. 10(a) is obtained. The forward coercivity $H_{c2,ea}$ is increased. No sign of a two step magnetization process is visible. In Fig. 10(f) the magnetic reversal process, now back at 0.2 Hz, reveals a change of sign of $H_{eb,ea}$. Also the coercivity $H_{c,ea}$ is reduced, significantly. This can be understood from the magnetic history of the sample, which has seen negative field values for several hours at the end of the measurement of Fig. 10(e). This results in an effective reverse of exchange bias due to the slowly rotating parts in the AF layer. This indicates that the forward and backward part of the loop in Fig. 10(e) correspond to different $H_{eb,ea}$ values for both loop branches due to the rotatable anisotropy part in the AF. The loop shift for the forward and backward part of the loop effectively differs. The changes relate directly to the rotatable anisotropy in the AF layer.

V. SUMMARY AND CONCLUSIONS

Exchange bias and rotatable anisotropy fields are separated by transversal pulse measurements in the subnanosecond time regime. From the magnetic damping parameter α_{eff} we find the onset of antiferromagnetic ordering at about $t_{IrMn}=1.0$ nm, before the onset of rotatable and unidirectional anisotropy. Rotatable anisotropy develops above $t_{IrMn}=1.4$ nm and exists up to the largest investigated AF layer thickness ($t_{IrMn}=8.7$ nm). The onset of exchange bias happens at $t_{IrMn}=2.0$ nm, the maximum is reached at about $t_{IrMn}=4.0$ nm.

The coupled F/AF system is characterized by both, the unidirectional and the rotatable anisotropy. Both contributions have to be taken into account, characterizing the F/AF layer interaction at finite temperatures. As one part of the AF is fixed and the other rotates time dependent, different degree of disordering in the AF layer occurs for each branch of the

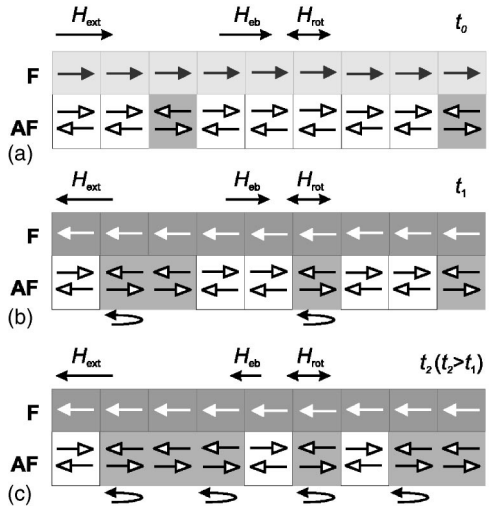

FIG. 11. (a) Initial spin configuration in the F/AF layer (schematic). (b) Magnetization configuration after reversing the magnetization in the F layer. (c) With increasing (measuring) time ($t_1 < t_2$) more AF grains reverse magnetization, the exchange bias field changes sign. Effective field direction and the rotating parts of the AF layer are indicated.

hysteresis loop [compare Fig. 11(a) with 11(b)]. Depending on the experimental time, the AF layer switches to a higher degree, the exchange bias field may realign opposite to the initial direction [Fig. 11(c)]. The AF switching leads to a discrepancy between loop shift and exchange bias field, comparing ultrafast susceptibility and quasistatic loop measurements. The rotatable parts in the AF layer are directly correlated to the coercivity field. The change of coercivity with t_{IrMn} is due to the rotating parts of the AF magnetization during reversal of the F layer. The dynamic switching character is confirmed by domain observation and magnetometry. The partial rearrangement in the AF layer is the source for the often reported loop asymmetries.[37–39,43,44] In particular in Refs. 39 and 44 the coexistence of asymmetry and ripple effects in the F were reported and related to partial remagnetization in the AF.

A peak of total anisotropy occurs at $t_{\mathrm{IrMn}} = 2$ nm. With further increasing AF layer thickness, the overall anisotropy decreases. This is presumably due to increasing perpendicular AF domain wall energy and the formation of partial planar domain walls in the AF layer at larger thickness.

A model describing the shown behavior must incorporate relaxation effects together with partial switching in the AF and needs to include perpendicular walls or disordering in the AF layer.[7,12,13,22] Our data is in qualitatively agreement with the model proposed by Stiles and McMichael.[22] In experiments, the time constant of the measurement technique used to investigate the F/AF interaction will dramatically change the results and has to be taken into consideration interpreting the experimental data.

ACKNOWLEDGMENTS

The authors thank W. Michalke and K. Kirsch for sample deposition. We also thank R. Schäfer for critically reading the manuscript and K. Steenbeck for helpful discussions.

*Electronic address: j.mccord@ifw-dresden.de

[1] W. H. Meiklejohn and C. P. Bean, Phys. Rev. **102**, 1413 (1956).
[2] M. Stiles and R. McMichael, Phys. Rev. B **59**, 3722 (1999).
[3] A. Berkowitz and K. Takano, J. Magn. Magn. Mater. **200**, 552 (1999).
[4] J. Nogues and I. K. Schuller, J. Magn. Magn. Mater. **192**, 203 (1999).
[5] R. L. Stamps, J. Phys. D **33**, R247 (2000).
[6] D. Mauri, H. C. Siegmann, P. S. Bagus, and E. Kay, J. Appl. Phys. **62**, 3047 (1987).
[7] A. P. Malozemoff, J. Appl. Phys. **63**, 3874 (1988).
[8] T. C. Schulthess and W. H. Butler, J. Appl. Phys. **85**, 5510 (1999).
[9] K. Takano, R. Kodama, A. Berkowitz, W. Cao, and G. Thomas, Phys. Rev. Lett. **79**, 1130 (1997).
[10] R. C. L. Wee, and R. L. Stamps, J. Appl. Phys. **89**, 6913 (2001).
[11] N. C. Koon, Phys. Rev. Lett. **78**, 4865 (1996).
[12] U. Nowak, A. Misra, and K. D. Usadel, J. Appl. Phys. **89**, 7269 (2001).
[13] D. Suess, M. Kirschner, T. Schrefl, J. Fidler, and R. Stamps, Phys. Rev. B **67**, 054419 (2003).
[14] J. R. L. de Almeida and S. Rezende, Phys. Rev. B **65**, 092412 (2002).
[15] H. Xi and R. M. White, Phys. Rev. B **61**, 80 (2000).
[16] Z. Quian, J. M. Sivertsen, and J. H. Judy, J. Appl. Phys. **83**, 6825 (1998).
[17] C. Leighton, J. Nogues, B. J. Jösson-Akerman, and I. K. Schuller, Phys. Rev. Lett. **84**, 3466 (2000).
[18] R. D. McMichael, M. D. Stiles, P. J. Chen, and W. F. Egelhoff, Phys. Rev. B **58**, 8605 (1998).
[19] R. J. Prosen, J. O. Holmen, and B. E. Gran, J. Appl. Phys. **32**, 91S (1961).
[20] M. S. Cohen, J. Appl. Phys. **33**, 2968 (1962).
[21] E. Fulcomer and S. H. Charap, J. Appl. Phys. **43**, 4190 (1972).
[22] M. D. Stiles and R. D. McMichael, Phys. Rev. B **63**, 064405 (2001).
[23] C. Schlenker, S. Parkin, J. Scott, and K. Howard, J. Magn. Magn. Mater. **54–57**, 801 (1986).
[24] H. Xi, R. White, S. Mao, G. Zheng, Y. Zhijun, and E. Murdock, Phys. Rev. B **64**, 184416 (2001).
[25] C. Leighton, M. R. Fitzsimmons, P. Yashar, A. Hoffmann, J. Nogués, J. Dura, C. F. Majkrzak, and I. K. Schuller, Phys. Rev. Lett. **86**, 4394 (2001).
[26] T. Zhao, H. Fujiwara, K. Zhang, C. Hou, and T. Kai, Phys. Rev. B **65**, 014431 (2001).
[27] M. M. Ali, C. H. Marrows, and B. J. Hickey, Phys. Rev. B **67**, 172405 (2003).
[28] K. Steenbeck, R. Mattheis, and M. Diegel, J. Magn. Magn. Mater. **279**, 317 (2004).
[29] T. J. Silva, C. S. Lee, T. M. Crawford, and C. T. Rogers, J. Appl.

Phys. **85**, 7849 (1999).
[30] R. D. McMichael, C. G. Lee, M. D. Stiles, F. G. Serpa, and P. J. Chen, J. Appl. Phys. **87**, 6406 (2000).
[31] E. Feldtkeller, Z. Phys. **176**, 510 (1963).
[32] G. Suran, H. Ouahmane, I. Iglesias, M. Rivas, J. Corrales, and M. Contreras, J. Appl. Phys. **76**, 1749 (1994).
[33] L. Spinu, A. Stancu, Y. Kubota, G. Ju, and D. Weller, Phys. Rev. B **68**, 220401 (2003).
[34] G. Sandler, H. Bertram, T. J. Siva, and T. Crawford, J. Appl. Phys. **85**, 5080 (1999).
[35] C. Kittel, Phys. Rev. **73**, 155 (1948).
[36] P. Miltényi, M. Gryters, G. Güntherodt, J. Nogués, and I. K. Schuller, Phys. Rev. B **59**, 3333 (1999).
[37] M. R. Fitzsimmons, P. Yashar, C. Leighton, I. K. Schuller, J. Nogués, C. F. Majkrzak, and J. A. Dura, Phys. Rev. Lett. **84**, 3986 (2000).
[38] V. I. Nikitenko, V. S. Gornakov, L. M. Dedukh, Y. P. Kabanov, A. F. Khapikov, A. J. Shapiro, R. D. Shull, A. Chaiken, and R. P. Michel, Phys. Rev. B **57**, R8111 (1998).
[39] J. McCord, R. Mattheis, and R. Schäfer, J. Appl. Phys. **93**, 5491 (2003).
[40] J. Geshev, L. G. Pereira, and J. E. Schmidt, Phys. Rev. B **66**, 134432 (2002).
[41] M. Ali, C. H. Marrows, M. Al-Jawad, B. J. Hickey, A. Misra, U. Nowak, and K. D. Usadel, Phys. Rev. B **68**, 214420 (2003).
[42] F. Nolting, A. Scholl, J. Stöhr, J. Seo, J. Fompeyrine, H. Siegwart, J.-P. Locquet, S. Anders, J. Lüning, E. Fullerton *et al.*, Nature (London) **405**, 767 (2000).
[43] Y. Wang, A. Petford-Long, T. Hughes, H. Laidler, K. O'Grady, and M. Kief, J. Magn. Magn. Mater. **242–245**, 1073 (2002).
[44] P. Gogol, J. Chapman, M. Gillies, and F. Vanhelmont, J. Appl. Phys. **92**, 1458 (2002).